XMCD for Monitoring Exchange Interactions. The Role of the Gd 4f and 5d Orbitals in Metal−Nitronyl Nitroxide Magnetic Chains

ARTICLE *in* JOURNAL OF THE AMERICAN CHEMICAL SOCIETY · AUGUST 2003

Impact Factor: 12.11 · DOI: 10.1021/ja034608u · Source: PubMed

J|A|C|S
ARTICLES
Published on Web 06/12/2003

XMCD for Monitoring Exchange Interactions. The Role of the Gd 4f and 5d Orbitals in Metal-Nitronyl Nitroxide Magnetic Chains

Guillaume Champion,[†,‡] Nikolia Lalioti,[§,⊥] Vassilis Tangoulis,[§,⊥] Marie-Anne Arrio,[∥] Philippe Sainctavit,[‡,∥] Françoise Villain,[†,‡] Andrea Caneschi,[§] Dante Gatteschi,[§] Christine Giorgetti,[‡] François Baudelet,[‡] Michel Verdaguer,[†] and Christophe Cartier dit Moulin*[,†,‡]

Contribution from the Laboratoire de Chimie Inorganique et Matériaux Moléculaires, Université Pierre et Marie Curie, Bât. F74, Case 42, 4 place jussieu, 75252 Paris Cedex 05, France, LURE, Université Paris-Sud, Bât 209D, BP 34, 91898 Orsay Cedex, France, Dipartmento di Chimica, Università degli Studi di Firenze, and UdR I.N.S.T.M. di Firenze, Via della Lastruccia 3, 50019 Sesto Fiorentino (Fi), Italy, and Laboratoire de Minéralogie Cristallographie de Paris, Université Pierre et Marie Curie, Tour 16, 4 place jussieu, 75252 Paris Cedex 05, France

Received February 11, 2003; E-mail: cartier@ccr.jussieu.fr

Abstract: We report here the X-ray magnetic circular dichroism (XMCD) study at the Gd $M_{4,5}$- and $L_{2,3}$-edges of two linear magnetic chains involving Gd(III) cations bridged by nitronyl nitroxide radicals. This spectroscopy directly probes the magnetic moments of the 4f and 5d orbitals of the gadolinium ions. We compare macroscopic magnetic measurements and local XMCD signals. The $M_{4,5}$-edges results are in agreement with the *J* values extracted from the fits of the SQUID magnetic measurements. The $L_{2,3}$-edges signals show that the electronic density in the Gd 5d orbitals depends on the neighbors of the gadolinium cations. Nevertheless, the 5d orbitals do not seem to play any role in the superexchange pathway between radicals through the metal ion proposed to explain the particular magnetic exchange interactions between the radicals in these chains.

Introduction

One-dimensional systems can in principle give rise to competing interactions when the spins are coupled antiferromagnetically to their next-nearest neighbors (nnn) independent of the sign of the interaction with the nearest neighbors (nn). To interpret the magnetic properties, it is necessary to take into account the nn and nnn interactions, which can be sometimes predominant. In the course of our investigation of magnetic materials containing exchange-coupled rare-earth ions and organic radicals,[1−7] we synthesized the linear chain compounds $Gd(hfac)_3NITR$ (hfac = hexafluoroacetylacetonate; NITR = 2-(*R*)-4,4,5,5-tetramethyl-4,5-dihydro-1*H*-imidazolyl-1-oxy 3-oxide) with R = isopropyl for **1**[8−10] and R = methoxyphenyl for **2**. They are one-dimensional alternating spin materials because NITR consists of organic bidentate radicals with spin $s = {}^1/_2$ which alternate along the chain with rare-earth Gd(III) magnetic ions with spin $S = {}^7/_2$ (the spin values are given in $\hbar$ units).

Despite rather small structural differences between the two radicals, they exhibit different magnetic properties. In **1**, the SQUID measurements[9] show a predominant nnn antiferromagnetic coupling between the two radicals ($J_2/k = -4.5$ K), despite the long distance between them, a weak nn ferromagnetic coupling between the Gd(III) cation and the radical ($J_1/k = 1.85$ K), and a weak nnn antiferromagnetic coupling between the gadolinium ions ($J_3/k = -0.33$ K). The three exchange pathways for **1** and **2** are schematized in Figure 1.

The nnn interactions between radicals are predominant, and this situation leads to a magnetic spin frustration because all of

† Laboratoire de Chimie Inorganique et Matériaux Moléculaires, Université Pierre et Marie Curie.
‡ Université Paris-Sud.
§ Università degli Studi di Firenze.
∥ Laboratoire de Minéralogie Cristallographie de Paris, Université Pierre et Marie Curie.
⊥ Present address: Department of Materials Science, University of Patras, 26504 Patras, Greece.

(1) Caneschi, A.; Gatteschi, D.; Laugier, J.; Rey, P. *J. Am. Chem. Soc.* **1987**, *109*, 2191.
(2) Caneschi, A.; Gatteschi, D.; Rey, P.; Sessoli, R. *Inorg. Chem.* **1988**, *27*, 1756.
(3) Caneschi, A.; Gatteschi, D.; Renard, J. P.; Rey, P.; Sessoli, R. *Inorg. Chem.* **1989**, *28*, 2940.
(4) Benelli, C.; Caneschi, A.; Gatteschi, D.; Pardi, L.; Rey, P. *Inorg. Chem.* **1989**, *28*, 275.
(5) Benelli, C.; Caneschi, A.; Gatteschi, D.; Sessoli, R. *Adv. Mater.* **1992**, *4*, 504.
(6) Benelli, C.; Caneschi, A.; Gatteschi, D.; Sessoli, R. *Inorg. Chem.* **1993**, *32*, 4797.
(7) Gatteschi, D. *Magnetic Molecular Materials*; NATO ASI Series E Vol. 198; Kluwer: Dordrecht, 1991.
(8) Benelli, C.; Caneschi, A.; Gatteschi, D.; Pardi, L.; Rey, P. *Inorg. Chem.* **1990**, *29*, 4223.
(9) Bartolomé, F.; Bartolomé, J.; Benelli, C.; Caneschi, A.; Gatteschi, D.; Paulsen, C.; Pini, M. G.; Rettori, A.; Sessoli, R.; Volokitin, Y. *Phys. Rev. Lett.* **1996**, *77*, 382.
(10) Affronte, M.; Caneschi, A.; Sussi, C.; Gatteschi, D.; Lasjaunias, J. C.; Paulsen, C.; Pini, M. G.; Rettori, A.; Sessoli, R. *Phys. Rev. B* **1999**, *59*, 6282.

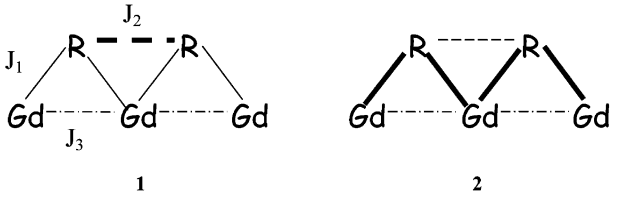

Figure 1. Scheme of the magnetic exchange interaction pathways in **1** and **2**. The thick lines represent the predominant exchange interaction.

the different exchange interactions cannot be fulfilled simultaneously. For **2**, we have found a predominant nn ferromagnetic coupling between the Gd(III) cations and the radicals (J_1/k = 6.8 K), a weak nnn antiferromagnetic coupling between the two radicals (J_2/k = −1.6 K), and a weak nnn antiferromagnetic coupling between the nearest gadolinium centers ions (J_3/k = −0.8 K). For **2**, the nn interactions between radicals and gadolinium cations are predominant, and this situation leads to a ferromagnetic state in which all of the spins tend to align parallel to the applied magnetic field.

For both compounds, the ferromagnetic interaction between the gadolinium cation and the radical was also confirmed by magnetic data of reference molecules built with one Gd^{III} coupled to one NITR radical.[11] For this exchange interaction, a model has already been proposed which involves the transfer of a fraction of an electron from the SOMO of the radical into an empty orbital of gadolinium.[12] This fraction of unpaired electron would polarize the unpaired electrons of the inner 4f orbitals, thus giving rise to a parallel alignment of the spins. The empty orbitals can be either the 6s or the 5d of the gadolinium ion.[13] To explain the strong nnn antiferromagnetic exchange interaction for **1**, different hypotheses have been proposed, including superexchange mechanisms involving the 4f and/or 5d and 6s gadolinium orbitals.[6,8−10]

Although this proposal is feasible, no direct confirmation has been obtained so far. Among the possible techniques which can probe the exchange pathway, XMCD is particularly attractive. XMCD derives from X-ray absorption spectroscopy (XAS). It is an element and orbital selective magnetic probe that has recently been developed with synchrotron radiation.[14] A magnetic field is applied on the sample, and we select one circular polarization of the X-rays. When magnetic (or paramagnetic) samples are concerned, this magnetic field induces anisotropy because of the Zeeman effect. The consequence is that the probed element does not absorb in the same way circularly left and circularly right polarized light. The difference between those two absorption spectra is the dichroic signal, proportional to the local magnetic moment born by the absorber. Moreover, this technique is able to separate spin $\langle S_z \rangle$ and orbital $\langle L_z \rangle$ contributions to the total magnetic moment. The important feature of XMCD is that in principle it can investigate different edges, that is, monitor different orbitals, thus providing direct access to the possible exchange pathways.

The goal of our work is to investigate the accuracy of the proposed superexchange mechanism to explain the nnn predominant interaction between radicals in **1** and to try to understand the origin of the differences of the macroscopic magnetic properties between **1** and **2**. To do that, we report here an X-ray magnetic circular dichroism (XMCD) study of the chains **1** and **2** at the Gd $M_{4,5}$-edges ($3d^{10}4f^7 \rightarrow 3d^9 4f^8$ transitions, probe of the 4f Gd half-filled orbitals)[15] and $L_{2,3}$-edges ($2p^6 4f^7 5d^0 \rightarrow 2p^5 4f^7 5d^1$ transitions, probe of the 5d Gd orbitals).[16−19] These compounds were chosen inside the family of $Gd(hfac)_3$NITR products because **1** and **2** show the more pronounced antiferromagnetic and ferromagnetic behaviors, respectively.

Experimental Section

Chemical Synthesis. $Gd(hfac)_3 \cdot 2H_2O$ was prepared as previously described.[20] NITiPr and NITPhOMe radicals were prepared according to literature methods.[21] The two compounds studied in this work can be formulated as $Gd(hfac)_3$NITR (hfac = hexafluoroacetylacetonate; NIT = 2-(*R*)-4,4,5,5-tetramethyl-4,5-dihydro-1*H*-imidazolyl-1-oxy 3-oxide) with R = isopropyl for **1** and R = methoxyphenyl for **2**. Crystals of **1** were prepared as reported in ref 8. $Gd(hfac)_3$(NITPhOMe), **2**, was synthesized according to the following procedure: 1 mmol of the $Gd(hfac)_3 \cdot 2H_2O$ salt was dissolved in 60 mL of dry boiling *n*-heptane, and a solution of 1 mmol of the radical in 10 mL of dry chloroform was added. The final solution was left in ambient temperature for slow evaporation. Green elongated fine crystals were obtained after 1 day and well analyzed for $Gd(hfac)_3$(NITPhOMe), **2**. Anal. Calcd for $C_{29}F_{18}GdH_{22}N_2O_9$: C, 33.44; H, 2.13; N, 2.69. Found: C, 33.39; H, 2.07; N, 2.67.

Physical Measurements. The temperature dependence of the magnetic susceptibility of $Gd(hfac)_3$(NITPhOMe) was measured on polycrystalline powder sample with a Cryogenics S600 SQUID magnetometer with an applied field of 0.1 and 1.0 T and in the 2−300 K temperature range. Data were corrected with the standard procedure for the contribution of the sample holder and of the diamagnetism of the sample. Magnetization measurements were performed at 2 K and in the 0−6.5 T field range.

XAS Data Collection and Processing. Gd $M_{4,5}$-Edges. X-ray absorption near the edge structures (XANES) and XMCD spectra were recorded on the soft X-ray SU22 beam line of the Super-ACO storage ring at LURE (Orsay).[22] The white beam was monochromatized using a YB66 double crystal monochromator. The samples were cooled to 2 K with an external magnetic field H varying from 0 to 6 T. During XMCD measurements, right circularly X-ray photons are selected. A first spectrum is recorded with the magnetic field parallel to the propagation vector of the photons, and a second one is recorded after having reversed the magnetic field. The XMCD signal is the difference between the two spectra.

Gd $L_{2,3}$-Edges. XANES measurements were performed at room temperature in transmission mode at the hard X-ray XAS 13 beamline of the DCI storage ring of LURE (Orsay)[23] using a Si 311 double crystal monochromator. XMCD spectra were recorded at the hard X-ray energy

(11) Benelli, C.; Caneschi, A.; Fabretti, A. C.; Gatteschi, D.; Pardi, L. *Inorg. Chem.* **1990**, *29*, 1753.
(12) Benelli, C.; Caneschi, A.; Gatteschi, D.; Pardi, L.; Rey, P. *Inorg. Chem.* **1989**, *28*, 3230.
(13) Guillou, O.; Bergerat, P.; Kahn, O.; Bakalbassis, E.; Boubeker, K.; Batail, P.; Guillot, M. *Inorg. Chem.* **1992**, *31*, 110.
(14) Brouder, C.; Kappler, J. P. In *Magnetism and Synchrotron Radiation*; Beaurepaire, E., Carrière, B., Kappler J. P., Eds.; Editions de Physique: Les Ulis (France), 1997; p 19.
(15) Goedkoop, J. B.; Thole, B. T.; van der Laan, G.; Sawatzky, G. A.; de Groot, F. M. F.; Fuggle, J. C. *Phys. Rev. B* **1988**, *37*, 2086.
(16) (a) Goedkoop, J. B.; Rogalev, A.; Rogaleva, M.; Neumann, C.; Goulon, J.; van Veenendaal, M.; Thole, B. T. *J. Phys. IV France* **1997**, *7*, 415. (b) Neumann, C.; Hoogenboom, B. W.; Rogalev, A.; Goedkoop, J. B. *Solid State Commun.* **1999**, *110*, 375.
(17) van Veenendaal, M.; Goedkoop, J. B.; Thole, B. T. *J. Electron Spectrosc. Relat. Phenom.* **1997**, *86*, 151.
(18) van Veenendaal, M.; Goedkoop, J. B.; Thole, B. T. *Phys. Rev. Lett.* **1997**, *78*, 1162.
(19) van Veenendaal, M.; Benoist, R. *Phys. Rev. B* **1998**, *58*, 3741.
(20) (a) Richardson, M. F.; Wagner, D. F.; Sands, D. E. *J. Inorg. Nucl. Chem.* **1968**, *30*, 1275. (b) Lamchen, M.; Wittay, T. W. *J. Chem. Soc. C* **1966**, 2300.
(21) Arrio, M.-A.; Scuiller, A.; Sainctavit, P.; Cartier dit Moulin, C.; Mallah, T.; Verdaguer, M. *J. Am. Chem. Soc.* **1999**, *121*, 6414.
(22) Ullman, F. E.; Osieky, J. E.; Boocock, D. G.; Darcy, R. *J. Am. Chem. Soc.* **1972**, *94*, 7049.

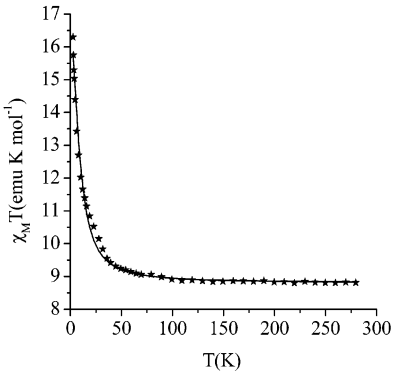

Figure 2. Temperature dependence of the magnetic susceptibility in the form of χ_MT vs T in the 2−300 K temperature range. The solid line represents the best fit according to eq 1. See text for details.

dispersive absorption line D11 of the DCI ring[24] at $T = 14$ K and $H = 1.8$ T. The isotropic spectra were normalized, and the XMCD signals presented here can be directly compared.

Ligand Field Multiplet Calculations. The Gd $M_{4,5}$-edges were calculated using the ligand field multiplet code developed by Thole[25] in the framework established by Cowan[26] and Butler.[27] This approach takes into account all of the electronic Coulombic repulsions, the spin−orbit coupling on every shell, and, even if this was not required for this study, treats the geometrical environment of the absorbing atom as a crystal field potential.[28] Once the parameters are well adjusted to reproduce the experimental XANES and XMCD spectra, one can extract from these calculations $\langle L_z \rangle$ and $\langle S_z \rangle$ of the probed orbitals.

Results and Discussion

Magnetic Studies of Gd(hfac)$_3$(NITPhOMe), 2. The temperature dependence of χ_MT of compound **2** is shown in Figure 2.

To fit the experimental data, we performed numerical transfer matrix calculations of the thermodynamic properties for a 1D magnet with spins (S,s) alternating along the chain, subject to competing nn ferromagnetic ($J_1 > 0$) and nnn antiferromagnetic ($J_2 < 0$ and $J_3 < 0$) exchange interactions,[8] with the spin Hamiltonian

$$H = -J_1 \sum_{n=1}^{N/2} (S_{2n-1} \cdot s_{2n} + s_{2n} \cdot S_{2n+1}) - J_2 \sum_{n=1}^{N/2} (s_{2n} \cdot s_{2n+2}) - J_3 \sum_{n=1}^{N/2} (S_{2n-1} \cdot S_{2n+1}) - g\mu_B H \sum_{n=1}^{N/2} S^x_{2n+1} - g'\mu_B H \sum_{n=1}^{N/2} s^x_{2n} \quad (1)$$

where S_{2n+1} represents a gadolinium spin, and s_{2n} represents a radical spin. We take periodic boundary conditions $s_{2n} = s$, $S_{2n+1} = S$. To limit the amount of calculations, the spins were approximated by classical planar rotators in the $x-y$ plane (perpendicular to the chain direction) where a magnetic field H is applied. The result of the fitting process for **2** is shown as a solid line in Figure 2, while the obtained values are $J_1/k = 6.8$ K, $J_2/k = -1.6$ K, $J_3/k = -0.8$ K. The analogous magnetic studies on **1**, previously reported, provided the following values: $J_1/k = 1.85$ K, $J_2/k = -4.5$ K, $J_3/k = -0.33$ K.

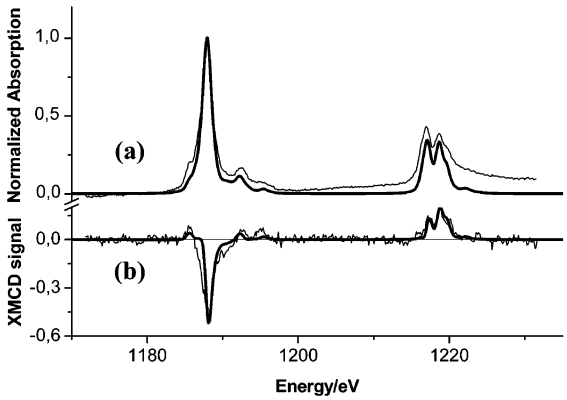

Figure 3. (a) Experimental (thin line) and calculated (thick line) isotropic spectra for **1** at the Gd $M_{4,5}$-edges ($T = 2$ K, $H = 6$ T). (b) XMCD experimental (thin line) and calculated (thick line) signals normalized to 100% circular polarized light.

XAS at Gd $M_{4,5}$-Edges. The experimental isotropic XANES and dichroic signals of **1** at the $M_{4,5}$-edges of gadolinium are displayed in Figure 3.

The general shape and the structures of these signals (position in energy, relative intensities) are characteristic of Gd^{III} ions.[15] The multiplet calculations of isotropic and XMCD spectra for **1** are also reported in Figure 3. For **2**, the isotropic spectra are the same, and the dichroic ones present the same shape and differ only in intensity. Therefore, we used the same parameters to simulate the experimental data for the two compounds: reduction factor of the Slater integrals $\kappa = 0.8$, no crystal field parameter, and 3d and 4f spin−orbit coupling constant values calculated for the free ion ($\xi_{4f} = 0.197$ eV for the states deriving from the initial configuration and $\xi_{3d} = 12.4$ eV and $\xi_{4f} = 0.225$ eV for the states deriving from the final configuration). We obtained a good agreement between calculated and experimental data since every structure is well reproduced in energy position and intensity for the isotropic spectra as well as for the XMCD spectra. This good agreement was expected because multiplet calculations are well adapted to describe transitions toward localized states. The lanthanide contraction makes the 4f orbitals of the cations atomic-like with negligible influence of the local environment. This localized character of the final state is consistent with the small reduction factor of the Slater integrals and the absence of crystal field parameter in the fitting procedure.

One can extract from the multiplet calculations accurate $\langle S_z \rangle_{4f}$ and $\langle L_z \rangle_{4f}$ values, which are, respectively, −3.47 and −0.03 (in $\hbar$ units). The very weak $\langle L_z \rangle_{4f}$ value is consistent with the $4f^7$ electronic configuration associated to the ^{8}S ground spectroscopic term for which no orbital momentum appears.

Moreover, the integrated area of XMCD signals is directly proportional to the magnetic moment of the probed 4f orbitals.[29] The evolution of these integrated areas versus the applied magnetic field for **1** and **2** is reported in Figure 4.

(23) Bleuzen, A.; Lomenech, C.; Escax, V.; Villain, F.; Varret, F.; Cartier dit Moulin, C.; Verdaguer, M. *J. Am. Chem. Soc.* **2000**, *122*, 6648.
(24) Champion, G.; Escax, V.; Cartier dit Moulin, C.; Bleuzen, A.; Villain, F.; Baudelet, F.; Dartyge, E.; Verdaguer, M. *J. Am. Chem. Soc.* **2001**, *123*, 12544.
(25) Thole, B. T.; Van der Laan, G.; Fuggle, J. C.; Sawatzky, G. A.; Karanatak, R. C.; Esteva, J.-M. *Phys. Rev. B* **1985**, *32*, 5107.
(26) Cowan, R. D. *The Theory of Atomic Structure and Spectra*; University of California Press: Berkeley, 1981.
(27) Butler, P. H. *Point Group Symmetry, Applications, Methods and Tables*; Plenum: New York, 1991.
(28) Van der Laan, G.; Kirkman, I. W. *J. Phys.* **1992**, *4*, 4189.
(29) Altarelli, M.; Sainctavit, P. In *Magnetism and Synchrotron Radiation*; Beaurepaire, E., Carrière, B., Kappler, J. P., Eds.; Editions de Physique: Les Ulis, 1997; p 65.

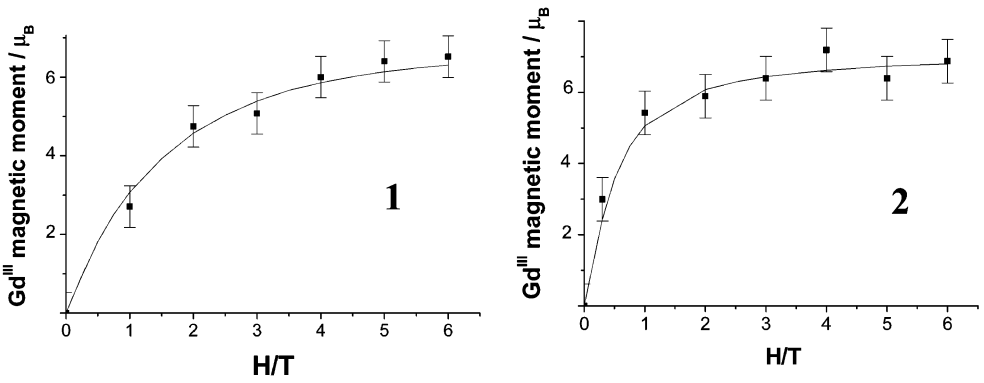

Figure 4. Experimental XMCD integrated area at the Gd M_5-edge vs H (■) for **1** and **2** as compared to the experimental magnetization curves (line) (T = 2 K).

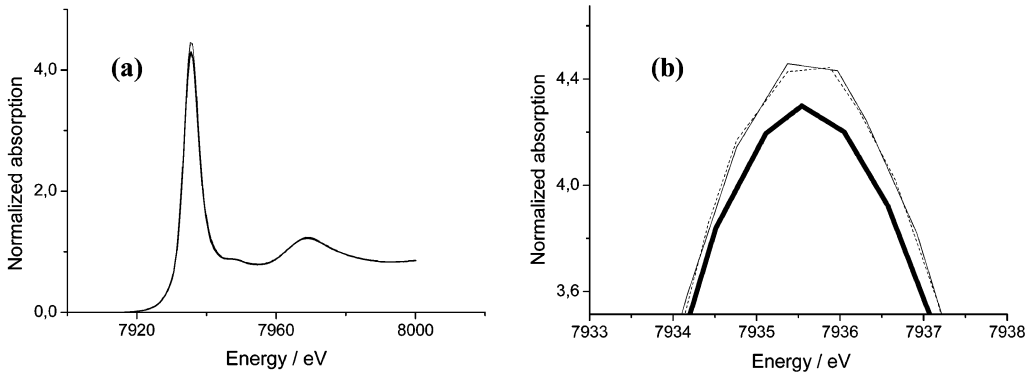

Figure 5. (a) XANES spectra at the L_2-edge for **1** (thin line), **2** (dotted line), and the $Gd(hfac)_3(H_2O)_2$ compound (thick line); (b) zoom on the absorption maximum.

The integration was done at the M_5-edge, and we checked that similar results were obtained at the M_4-edge. The error bar was evaluated taking into account the experimental signal/noise ratio. The dichroic signal increases for both compounds when the applied magnetic field increases. This is correlated with the progressive alignment of the magnetic moments of the 4f orbitals of the gadolinium cations in the direction of the applied magnetic field. The macroscopic magnetization curves of **1** and **2** recorded with a SQUID magnetometer at T = 2 K are also reported in Figure 4. Because the integrated areas of the XMCD signals are proportional to the local magnetic moments of the probed orbitals of the probed ion, the experimental dots and the macroscopic magnetization curve have been arbitrarily scaled to 7 μ_B per gadolinium ion at saturation. For both compounds, we observe a good agreement between the macroscopic magnetic data and the local data. This means that the local magnetization of the 4f orbitals of the Gd^{III} cations follows that of the whole chain. This is the first time that such a study has been led on gadolinium molecular systems and such local magnetization curves are obtained.

The local magnetic moment of the 4f orbitals of the gadolinium reaches saturation more slowly for **1** than for **2**. Compound **2** for which the nn predominant interactions between Gd and radicals are expected to be ferromagnetic reaches saturation faster. For **1**, the nnn predominant antiferromagnetic interactions between radicals lead to a magnetic spin frustration, and the saturation is more difficult to reach. XMCD results confirm the nature of the dominant interactions obtained by the fitting procedures of the macroscopic magnetization curves.

Finally, the similar 4f electronic structure of **1** and **2** evidenced by the use of the same multiplet parameters set shows that the Gd 4f orbitals probably do not play a role in the difference of the macroscopic magnetic properties observed between the two chains. The next step is now to probe the 5d orbitals of the Gd^{III} cations, more delocalized than the 4f and thus more likely to participate in the nnn predominant radical−radical superexchange pathway in **1**, as proposed in ref 8.

XAS at the Gd $L_{2,3}$-Edges. The L_2 XANES spectra of **1** and **2** are reported in Figure 5.

The absorption maximum at 7935.5 eV corresponds to the $2p^64f^75d^0 \rightarrow 2p^54f^75d^1$ transitions, authorized by the selection rules in the electric dipolar approximation. The integrated area of this feature (and, in first approximation, its intensity) reflects the Gd 5d empty state density. At higher energies, the features correspond to transition toward states of the ionization continuum. If a direct overlap between the nearly atomic 4f orbitals of the Gd ions and the surrounding molecular orbitals is not very likely, an interatomic hybridization of the 5d orbitals with the ligand orbitals is expected. So, the intensity of the absorption maximum will be sensitive to the donor (or acceptor) electronic character of the ligands around the rare-earth. The XANES spectra of **1** and **2** are rigorously superimposable to each other. The same result is obtained at the L_3-edge, not shown here. That means that the electronic structure and more precisely the 5d empty state density of the Gd ions are the same for the two chains and do not depend on the nature of the substituent on the nitronyl nitroxide bridging radical.

In the $Gd(hfac)_3(H_2O)_2$ compound, the two oxygen atoms from water molecules take the place of the oxygen atoms coming from the radicals in **1** and **2**. We observe a small but significant decrease of the intensity of the absorption maximum at the L_3-edge (inset of Figure 5), also observed at the L_2-edge. The Gd

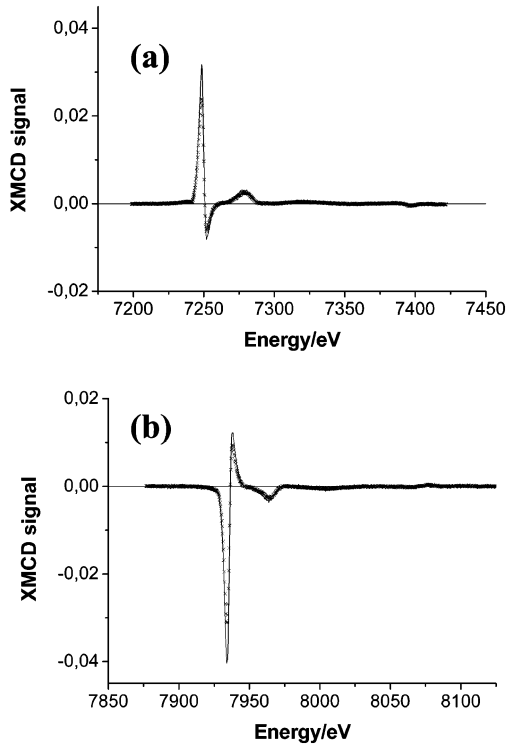

Figure 6. XMCD signals for **1** (×××) and **2** (thin line) recorded at the (a) L_3-edge; (b) L_2-edge.

5d empty state density is more important in the chains than in the $Gd(hfac)_3(H_2O)_2$ compound. This result confirms the expected more important electron donor character of the oxygen atoms of H_2O molecules than those of the radicals, and the more covalent nature of the $Gd-OH_2$ bonds.

Let us turn now to the XMCD signals. Very few experimental techniques are able to access the magnetism of the 5d orbitals, and XMCD at the $L_{2,3}$-edges provides a useful tool for studying directly the 5d magnetic moment. Nevertheless, the description of the XMCD at the rare-earth L-edges is complicated, and the shape and amplitude cannot yet be explained by a simple model.[16−18] The presence of a quadrupolar contribution ($2p \rightarrow 4f$) in the preedge region of the L_3-edge has also been identified.[30] The presence of 4f electrons leads to a 4f−5d intraatomic exchange interaction which induces the spin and orbital polarization of the 5d states.[31]

XMCD signals at the $L_{2,3}$-edges for **1** and **2** are reported in Figure 6.

The signals are represented without taking into account the polarization rate of the D11 beamline which is around 70%. The isotropic signals were normalized with an edge-jump of 1 at the L_3-edge and 0.5 at the L_2-edge which corresponds to the statistical branching ratio. The signals are comparable to signals obtained in Gd oxide insulators.[16] The most intense part of the dichroic signal is observed at the maximum of the isotropic spectrum, and it corresponds for **1** (**2**) to 2.4% (3.2%) of the isotropic spectrum at the L_3-edge and 6.2% (8.1%) at the L_2-edge. As previously observed, the $L_{2,3}$ XMCD spectra have line shapes that are close to the derivative of the XAS ones.[16] As expected, the sign of the dichroic signal is reversed at the L_3- and L_2-edges.[32] Quadrupolar transitions ($2p^6 4f^7 \rightarrow 2p^5 4f^8$) could occur in the low energy part of the L_3 isotropic and dichroic spectra.[16,30] Yet, as observed in previous studies,[16b] these transitions are of very low intensity because they only show up as a very small dip before the main dipolar contribution, and moreover they are well separated from the rest of the L_3 spectrum. Therefore, we have been able to integrate the dichroic signal without the quadrupolar contribution. The shape of the XMCD signals is the same for the two compounds. The higher intensity of the signal for **2** indicates its faster reaching of saturation previously evidenced by the XMCD study at the $M_{4,5}$-edges. This result shows that the 5d-XMCD signal follows the 4f magnetic moment and that of the whole chain.

Table 1. Integrated Areas of Normalized XMCD Signals for **1** and **2**

	L_3 XMCD integrated area	L_2 XMCD integrated area
compound **1**	0.114	−0.141
compound **2**	0.144	−0.178

To go further and obtain quantitative results from XMCD signals, one can generally use the orbital[33] and spin[34] sum rules formulated as follows:[32]

$$\langle L_z \rangle = 2(\Delta L_3 + \Delta L_2)\frac{(10-n)}{\int_{L_3+L_2}(\mu^+ + \mu^- + \mu^0)}$$

and

$$\langle S_2 \rangle = \frac{3}{2}(\Delta L_3 - 2\Delta L_2)\frac{(10-n)}{\int_{L_3+L_2}(\mu^+ + \mu^- + \mu^0)} - 3.5\langle T_z \rangle$$

where ΔL_3 and ΔL_2 are the dichroic integrated areas at the L_3- and L_2-edges, respectively; n is the number of electrons in the valence shell; μ^+, μ^-, and μ^0 are the absorption coefficients for left circularly polarized light, right circularly polarized light, and light which is linearly polarized with the polarization vector parallel to the quantization axis; and T_z is the value of the magnetic dipole operator.

For a pure $5d^0$ ground state configuration, which is the case for Gd^{III} ions, these sum rules give $\langle L_z \rangle_{5d} = \langle S_z \rangle_{5d} = \langle T_z \rangle_{5d} = 0$.[16,18,30,31,33,34] We performed simple multiplet calculations using the $2p^6 5d^0$ ground state configuration and $2p^5 5d^1$ final state configuration, neglecting the 2p−4f and 5d−4f exchange interactions in the final state which are difficult to include in the calculations.[16a] We found that the integrated XMCD signals are equal to zero at the L_3- and L_2-edges.

The XMCD signal integrated areas A_{L2} and A_{L3} evaluated for **1** and **2** are reported in Table 1.

We can see that they are very different from zero, at all edges.

Following the $\langle L_z \rangle_{5d}$ sum rule, which does not require any assumption on the value of $\langle T_z \rangle$ (which is often a source of debate), $\langle L_z \rangle_{5d} = 0$ leads to $A_{L2}/A_{L3} = -1$, different from the

(30) Lang, J. C.; Srajer, G.; Detlefs, D.; Goldman, A. I.; Köhig, H.; Wang, X.; Harmon, B. N.; McCallum, R. W. *Phys. Rev. Lett.* **1995**, *74*, 4939.
(31) Fukui, K.; Ogasawara, H.; Kotani, A.; Harada, I.; Maruyama, H.; Kawamura, N.; Kobayashi, K.; Chaboy, J.; Marcelli, A. *Phys. Rev. B* **2001**, *64*, 104405.
(32) Sacchi, M. In *Magnetism and Synchrotron Radiation*; Beaurepaire, E.; Scheurer, F., Krill, G., Kappler, J. P., Eds; Springer-Verlag: Berlin, 2001; p 87.
(33) Thole, B. T.; Carra, P.; Sette, F.; van der Laan, G. *Phys. Rev. Lett.* **1992**, *68*, 1943.
(34) Carra, P.; Thole, B. T.; Altarelli, M.; Wang, X. *Phys. Rev. Lett.* **1993**, *70*, 694.

−1.24 value found for our systems. This would suggest that $\langle L_z \rangle_{5d} \neq 0$ in **1** and **2**, generally found to be equal to zero for the Gd^{III} ions.[35] However, in this case, these sum rules cannot be applied to obtain quantitative information for several reasons. First, we do not know the exact number of electrons in the 5d orbitals because of the possible delocalization on the ligands and/or because of their possible inner hybridization with 4f partially occupied orbitals. Second, we do not know the exact value of $\langle T_z \rangle$ even if this term, which is due to an anisotropy in the spin moment, is often taken equal to zero because of the nearly cubic symmetry around the rare-earth element. Finally, these sum rules were given considering that there were no interaction between the photoexcited 5d electron and the 4f electrons.[36] This is probably not the case in our systems, and there is no simple relation between the XMCD spectra and the 5d magnetic moment in the ground state. We cannot conclude on the presence/absence of an orbit moment born by the 5d orbitals.

Conclusion

We report here XANES and XMCD results at the Gd $M_{4,5}$- and $L_{2,3}$-edges obtained for two Gd-radical chains **1** and **2**, presenting different macroscopic magnetic properties.

The $M_{4,5}$ XMCD results show that the 4f orbitals follow the macroscopic magnetic properties of the sample. The 4f local moments reach saturation faster in **2** than in **1**, in agreement with SQUID measurements. Multiplet calculations confirm the localized character of the 4f orbitals and the quasi nullity of the orbital momentum of the 4f shell, as expected for the $4f^7$ configuration of the Gd^{III} cation. We do not observe any particular influence of the nature of the dominant exchange interaction pathway on the 4f orbitals, as expected for these quite-atomic orbitals.

Because the XANES spectra at the $L_{2,3}$-edges are rigorously superposable, the 5d empty state density is the same for **1** and **2**. As for the 4f orbitals, the predominant exchange interaction pathway, different for the two compounds, has no influence on the state density of the 5d shell. Moreover, we have shown in this study that the electron density in the gadolinium 5d orbitals was different when replacing water molecules by nitronyl nitroxide radicals. Therefore, the environment of the rare earth might have an influence on the spin density on the 5d gadolinium orbitals.

All of these results confirm the similarity of the 5d orbitals electronic structure for **1** and **2**, despite the differences of the macroscopic magnetic properties. This XMCD study does not allow one to evidence a particular role of the 5d Gd orbitals in the superexchange mechanism leading to the predominant (nnn) interaction between radicals in **1**.

Acknowledgment. This work was supported by grants and funds from E.U. Networks 3MD (ERBFMRX CT980181) and MOLNANOMAG (HPRN-CT-1999-00012), italian MIUR, and CNR.

JA034608U

(35) Giorgetti, C. Ph.D. Dissertation, Université Paris-Sud, Orsay, 1994.
(36) Wu, R.; Freeman, A. J. *Phys. Rev. Lett.* **1994**, *73*, 1994.